

# Behaviour of fresh and fouled railway ballast subjected to direct shear testing - A discrete element simulation

Buddhima Indraratna<sup>1</sup>, Ngoc Trung Ngo<sup>2</sup>, Cholachat Rujikiatkamjorn<sup>3</sup>, and J S Vinod<sup>4</sup>

## ABSTRACT

This paper presents the three-dimensional discrete element method (DEM) that was used to study the shear behaviour of fresh and coal fouled ballast in direct shear testing. The volumetric changes and stress-strain behaviour of fresh and fouled ballast were simulated and compared with the experimental results. 'Clump logic' in Particle Flow Code (PFC<sup>3D</sup>) incorporated in a MATLAB Code was used to simulate irregular shaped particles in which groups of ten to twenty spherical balls were clumped together in appropriate sizes to simulate ballast particles. Fouled ballast with various Void Contaminant Index (VCI), ranging from 20%VCI to 70%VCI, were modelled by injecting a specified number of miniature spherical particles into the voids of fresh ballast. The DEM simulation captures the behaviour of fresh and fouled ballast as observed in the laboratory showing that the peak shear stress of the ballast assembly decreases and the dilation of fouled ballast increases with an increasing of VCI. Furthermore, the DEM also provides insight to the distribution of contact force chains and particle displacement vectors, which cannot be determined experimentally. These micromechanical observations clearly justify the formation of a shear band and the evolution of volumetric changes during shearing. The reduced maximum contact force associated with increased particle contact area due to fouling explains the decreased breakage of fouled ballast. An acceptable agreement was found between the DEM model predictions and laboratory data.

<sup>1</sup> Professor of Civil Engineering, Faculty of Engineering,  
Research Director, Centre for Geomechanics and Railway Engineering, University of Wollongong, Wollongong City, NSW 2522, Australia  
Centre of Excellence in Geotechnical Science and Engineering, Australia  
Email: indra@uow.edu.au, Ph: +61 2 4221 3046 Fax: +61 2 4221 3238

<sup>2</sup> PhD Candidate, Faculty of Engineering,  
Centre for Geomechanics and Railway Engineering, University of Wollongong, Wollongong City, NSW 2522, Australia  
Email: ntn743@uowmail.edu.au, Ph: +61 2 4239 2359 Fax: +61 2 4221 3238

<sup>3</sup> Senior Lecturer, Faculty of Engineering,  
Centre for Geomechanics and Railway Engineering, University of Wollongong, Wollongong City, NSW 2522, Australia  
Centre of Excellence in Geotechnical Science and Engineering, Australia  
Email: cholacha@uow.edu.au, Ph: +61 2 4221 5852 Fax: +61 2 4221 3238

<sup>4</sup> Senior Lecturer, Faculty of Engineering,  
Centre for Geomechanics and Railway Engineering, University of Wollongong, Wollongong City, NSW 2522, Australia  
Centre of Excellence in Geotechnical Science and Engineering, Australia  
Email: vinod@uow.edu.au, Ph: +61 2 4221 4089 Fax: +61 2 4221 3238

## Introduction

The ballast layer plays a crucial part in transmitting and distributing the wheel load from sleepers to the underlying sub-ballast and subgrade at a reduced and acceptable level (Selig and Waters, 1994). Upon repeated train loading, ballast becomes degraded and fouled by the progressive accumulation of fines within the ballast voids. In Australia, ballast degradation, infiltration of external fine particles such as coal into the ballast, as well as pumping (liquefaction) of soft subgrade, decreases the void ratio (fouling), seriously decreasing the shear strength and drainage capacity of the track (Dombrow et al. 2009; Indraratna et al. 2010b). Feldman and Nissen (2002) stated that in a Queensland freight line, coal fines account for 70%-95% of contaminants followed by 5%-30% of fouling due to ballast breakage. Given the prolonged droughts and hot climate in Queensland, tracks fouled by coal are often relatively dry, but in the event of rainfall the resulting poor drainage due to fouling adversely affects their performance (Indraratna et al. 2011a).

The behaviour of fresh and fouled ballast has been investigated in the past (e.g. Indraratna and Salim 2002; Suiker et al. 2005; Anderson and Fair 2008; Aursudkij et al. 2009; Huang et al. 2009a; Indraratna et al. 2009; Indraratna et al. 2010a; Tutumluer et al. 2007; Tutumluer et al. 2008). However, most of these studies were conducted in the laboratory and only limited attempts were made to study the effects of fouling numerically. Furthermore, due to the discrete nature of ballast material, continuum modelling through finite element or finite difference methods is no longer realistic. They are unable to provide any insight into micro-scale responses such as contact force chain developed among the particles and the associated displacement vectors when subjected to shear loads. The discrete element method (DEM) based on discrete particle mechanics introduced by Cundall and Strack (1978) has progressed rapidly over the years and can now model the more insightful micro-mechanical behaviour of granular materials that cannot be examined experimentally (e.g. Sitharam and Vinod 2005; Lobo-Guerrero and Vallejo 2006; Lu and McDowell 2006; Hossain et al. 2007; Sitharam and Vinod 2008; Sitharam and Vinod 2009; Huang et al. 2009b; Thakur et al. 2010; Indraratna et al. 2010a; Wang and Gutierrez 2010; O'Sullivan et al. 2008; O'Sullivan and Cui 2009; O'Sullivan 2011; Stahl and Konietzky 2011), among others. The use of DEM to predict the stress-strain response of fouled ballast has been very limited in literature. Huang et al. (2009a, b) conducted an experimental and

DEM study, but they did not analyse the volumetric change of ballast in relation to various levels of fouling. This current study is an attempt to apply DEM to model both fresh and fouled ballast subjected to direct shear testing, to capture the volumetric change and corresponding stress-strain behaviour at various levels of fouling.

### Experimental program

A series of large-scale direct shear tests on 300mm × 300mm × 200mm size specimens were conducted. To minimise the boundary effects, slightly smaller ballast with a maximum particle size ( $d_{100}$ ) of 40mm were used rather than the  $d_{100}$  of 55-60mm used in typical Australian ballast gradations (Indraratna et al. 2011a). This gradation satisfied the size ratios discussed by Fagnoul and Bonnechere (1969), Marachi (1969), Indraratna et al. (1993, 2012). Moreover,  $D_{60}$  of the tested ballast is 20 mm. Therefore, at least 60% of ballast particles were 10 times smaller than the shear box dimensions. Past large-scale triaxial tests conducted by many researchers (e.g. Marsal, 1973; Indraratna et al., 1993) have shown that as long as the ratio of testing chamber dimension/particle size ratio is greater than 7-8 for the vast majority of particles, the boundary effects can be neglected. By sub-dividing the sample of ballast into small layers, predetermined amounts of coal fines (fouling material) were uniformly distributed into the void spaces to represent a given void contaminant index (VCI) as defined by Indraratna et al. (2010b):

$$VCI = \frac{1+e_f}{e_b} \times \frac{G_{s,b}}{G_{s,f}} \times \frac{M_f}{M_b} \times 100 \quad (1)$$

where  $e_f$  = void ratio of fouling material,  $e_b$  = void ratio of fresh ballast,  $G_{s,b}$  = specific gravity of ballast,  $G_{s,f}$  = specific gravity of fouling material,  $M_f$  = dry mass of fouling material,  $M_b$  = dry mass of fresh ballast.

The main advantage of Equation (1) is that it can include different types of fouling materials such as coal, mud, or pulverised ballast by incorporating their respective specific gravity ratio, unlike the previous methods of fouling assessment (e.g. Selig and Waters, 1994; Feldman and

Nissen, 2002). The particle size distribution of fresh and fouled ballast at various values of VCI is shown in Figure 1.

Large scale direct shear tests were conducted for fresh and fouled ballast at various levels of fouling, ranging from 0% to 95% VCI, at relatively low normal stresses ranging from 15kPa to 75kPa, to represent typical track conditions under low confinement (Lackenby et al. 2007). Each specimen was subjected to a maximum horizontal displacement of  $\Delta h=37\text{mm}$  (approximately 12.3% shear strain), which corresponds to the maximum movement allowed by the direct shear test apparatus. The experimental results of large-scale direct shear test were reported in detail by Indraratna et al. (2011a) and some of this data was used to compare with the current DEM analysis. The laboratory results show that the peak shear stress increased non-linearly, with an increase in normal stress, but then it decreased as the VCI increased. Indraratna et al. (2011a) attributed this to coal fines coating the surface of the ballast particles and thereby reducing the interlocking effect among the grains. In other words, the coal fines may act as a lubricant that facilitates the grains sliding and rolling over each other more easily, resulting in increased dilation.

### **Numerical simulation**

Particle Flow Code (PFC<sup>3D</sup>) has been developed based on the discrete element method (Cundall and Strack, 1979). The calculation cycle in PFC<sup>3D</sup> is a time stepping algorithm that utilises two successive cycles to calculate the contact forces and displacement of particles using Newton's second law of motion. The contact and body forces arising from the relative displacement at each contact are then updated by applying the force-displacement relationship (Itasca, 2008). The modelling of irregular shaped particles, model preparation, and the relevant micro-mechanical input parameters for the DEM simulation are discussed below.

### **Modelling the ballast assembly in DEM**

The entities representing the particles in PFC<sup>3D</sup> are spheres. Due to insufficient interlocking and inevitable excessive rolling, spherical units are usually unable to model granular particles that are

by nature, irregular or angular (Oda and Iwashita, 1999). Lim and McDowel (2005); Lu and McDowel (2007); Ferrellec and McDowel (2008); Thakur et al. (2010); Stahl and Konietzky (2011) have attempted to model the complex shapes of particles in DEM by 'clump logic', i.e. a method of forming irregular particles by connecting and overlapping a number of spheres of different sizes, and by assigning the corresponding radii and coordinates (Itasca, 2008). The clump behaves like a rigid body where the internal contacts are ignored. In this study, to model typical ballast shapes, nine distinct particle shapes with sizes ranging from 9.5mm to 40mm were introduced. The typical particle shapes selected from real ballast aggregates were mimicked by assembling a number of spherical balls as described by Indraratna et al. (2010a). The size of DEM particles was influenced by the largest dimension of each particle of ballast and its angularity. A sub-routine using MATLAB code was created to build particle templates. The data obtained from the sub-routine, including the radii and coordinates of spherical balls in a Cartesian system, were then exported to PFC<sup>3D</sup>. An additional sub-routine was written in FISH language to build a library of nine representative ballast shapes. Figure 2 shows the images of particle shapes generated for the DEM simulation.

### **DEM simulation of direct shear test**

A large scale shear box 300mm long  $\times$  300mm wide  $\times$  200mm high, and separated horizontally into two equal boxes, was simulated with rigid walls. A free loading plate that allowed the particles to be displaced vertically during shearing was placed on the top boundary. This plate was used to apply normal load and to monitor vertical displacement during shearing (specific effects of dilation within the shear box are not considered). The DEM model of this direct shear box for both fresh and fouled ballast (VCI=40%), is shown in Figure 3. A total of 8281 spherical particles with sizes ranging from 9.5mm to 40mm were generated in order to simulate actual ballast gradation (Figure 1). Irregular shaped particles were generated by 'clumping' using the sub-routines developed by the authors. Each spherical balls was then replaced by a clump with the same volume (e.g. 8281 clumps were generated). Particles were generated in the shear box at random orientations to resemble experimental conditions. The void ratio of the assembly representing the initial condition of the test specimen was controlled at 0.82 (i.e. porosity of 45%), similar to the ballast samples tested in the laboratory. By conducting calibration of a clump assembly subjected to large-scale direct shear test with experimental data reported by

Indraratna et al. (2011a), a set of micro-mechanical parameters adopted for DEM simulation of fresh ballast are given in Table 1. A linear contact model (e.g. linear elastic in both normal and tangential direction), following previous studies was used for the numerical simulations (e.g. Thakur et al. 2010; Indraratna et al. 2010a; McDowel et al. 2006).

The assembly was then cycled to reach equilibrium through facilitating particles to form contact with each other while keeping the void ratio of the assembly constant. The normal stress applied was kept constant by adjusting the position and velocity of the top plate using a numerical servo-control mechanism (Itasca, 2008). Similar to laboratory conditions (conducted shearing velocity in laboratory was 0.04 mm/second), the lower part of the shear box was allowed to move horizontally at a velocity of  $0.1 \times 10^{-4}$  mm/time step, while the upper section was fixed (Figure 4). The time step used in the simulations was  $1.9 \times 10^{-5}$ /second. This relatively low shearing rate was not enough to unduly disturb the assembly, but still attain an acceptable convergence rate (e.g. approximately 170 hours for simulation of fresh ballast and about 500 hours for 70%VCI fouled ballast). Each simulation was sheared to a horizontal displacement of 40mm (i.e., the maximum horizontal displacement observed in the tests). During shearing, the displacement of the top plate was recorded to determine the associated change in volume, and a sub-routine was developed to capture the resultant forces generated at the walls in the upper section of the shear box.

### Computational procedures

As shown in Figure 4, the shear force  $F_S$  can be calculated by considering the equilibrium of forces in a horizontal direction. The normal force  $F_N$  acting on the shear band is the sum of the applied normal load  $N$ , the weight of ballast in the upper box  $W_b$  and the weight of the top load plate  $W_p$ . Therefore, the shear force  $F_S$  and the normal force  $F_N$  acting on the horizontal shear plane can be calculated as follows:

$$F_S = \sum_{iw=1}^{N_{wall}} (N_{Y_{iw}} + S_{Y_{iw}}) \quad (2)$$

$$F_N = N + W_b + W_p \quad (3)$$

In the above,  $N_{Y_{iw}}$  is the normal force acting on the left and right hand side walls of the upper box, and  $S_{Y_{iw}}$  is the shear force acting on the upper box. The upper box has four walls and a top

plate, hence the total wall number  $N_{wall} = 5$ . The length and width of the shear box are  $L$  and  $B$ , respectively. If the box is sheared at a velocity of  $v$ , then at any time  $t$ , the contacted shearing area of the shear band incorporating the shear displacement is  $B(L-vt)$ . The normal and shear stresses are now readily computed as:

$$\sigma_n = \frac{F_N}{L(B-vt)} \quad (4)$$

$$\tau_{zy} = \frac{F_s}{L(B-vt)} \quad (5)$$

where  $\sigma_n$  and  $\tau_{zy}$  are the normal and shear stresses, respectively.

The bulk coefficient of friction is then calculated by:

$$\phi_b = \frac{\tau_{zy}}{\sigma_n} = \frac{F_s}{F_N} \quad (6)$$

## Numerical results and discussion

### Shear stress-strain and volumetric change analysis

DEM simulations were conducted to model fresh ballast subjected to three different normal stresses of 27 kPa, 51 kPa, and 75 kPa. The shear stress and volumetric changes were monitored during shearing. Figure 5 shows the plots of shear stress, shear strain, and volumetric strain obtained by DEM, compared to the laboratory data reported by Indraratna et al. (2011a). The predicted results at all normal stresses, agreed with the experimental results. The strain softening behaviour of ballast follows a similar trend with other rockfill aggregates of comparable sizes (e.g. Marsal, 1973; Indraratna et al. 1998; Charles and Watts, 1980). Volumetric dilation was also observed in all simulations, whereby the bigger the normal stress ( $\sigma_n$ ), the higher the peak stress and the smaller the dilation, as expected. The DEM analysis shows a noticeable discrepancy in stress-strain curves, i.e. markedly decreased stress and retarded dilation shown by the experimental data at a shear strain of 4-8% compared to the predicted line. This difference may be attributed to some particle degradation that could not be accurately captured in the DEM simulation and the rigidity of loading plate. Indeed, owing to the breakage of ballast aggregates, the reduction in shear strength would also be accompanied by a decrease in dilation (i.e.

increased compression of the assembly of smaller particles). Lackenby et al. (2007) also demonstrated that particle breakage would increase the compression of the granular assembly followed by increased in dilation upon further shearing, which is in agreement with the experimental data plotted in Figure 5. Similar behaviour is also observed in Figures 12-14 presented later for fouled ballast.

### **Contact force distribution and particle displacement**

Figure 6 presents the distribution of contact force chains at various shearing stages for a DEM simulated test with a normal stress of 51 kPa. Contact forces between particles were plotted as lines whose thickness is proportional to the magnitude of the force. Figure 6 shows 2D side view of the projection of all contact forces on vertical plane (YZ) and also illustrates how the applied load was transmitted within the particle assembly. At its initial state ( $\varepsilon_s=0\%$ ), the contact forces were distributed uniformly throughout the assembly and transmitted vertically from the top to the bottom of the shear box when normal stress was applied, but as shearing progressed, the contact forces intensified from the bottom left to the top right corner, as shown in Figures 6 (b)-(d). At the end of shearing, Figure 6d shows the lowest contact force magnitude compared to Figures 6b and 6c. This can be attributed to a reduction of coordination number (the average number of contacts per particle) associated with an increase in dilation of the ballast assembly, and the corresponding drop in shear strength (strain softening).

The evolution of displacement vectors at shear strains of 3% and 13% at an applied normal stress of 51kPa are presented in Figures 7a and 7b, respectively. At 3% shear strain (Figure 7a), while particles in the lower box displaced horizontally, particles in the upper box moved downwards causing densification (compression) of the granular assembly. On the other hand, at much higher shear strain (e.g. 13%), particles in the upper box tended to displace upwards (Figure 7b) causing dilation. These micro-mechanical observations clearly present the insightful evolution of volumetric changes during shearing within a granular medium, and the corresponding strain softening response where a continuum mechanics approach is unable to deliver the same level of clarity.

During the process of shear box testing, the shear plane usually propagates horizontally at low shear strains. However, at a relatively large shear strain  $> 10\%$ , the intensity of inter-particle

contact forces as determined by DEM tend to be inclined to the direction of shear strain (Fig. 7c). The DEM analysis shows that during shearing the particles of ballast at the rear of shear box displaced downwards while particles at the front displaced upwards. Volumetric strain was not distributed uniformly within the ballast assembly because dilation tends to occur at the front of the shear box and compression at the back as well as the overturning of loading plate was not considered. This can be attributed to a contact force chain that forms in the shear band where the particles within the shear band are displaced and rotate more than those outside the shear band (Cui and O'Sullivan, 2006 and Zhang and Thornton, 2007). In this aspect, our understanding of conventional shear plane propagation in relation to continuum mechanics is different to the micro-mechanical implications of potential shear banding governed by inter-particle movement, contact force distribution, and associated principal stress relationships. This disparity between continuum mechanics and micro-mechanics has been further elaborated on by Liu (2006), Wang et al. (2007) and O'Sullivan (2011).

#### **Further validation of the DEM model**

The same DEM model was validated by simulating the additional direct shear tests conducted at significantly higher normal stresses of 172 kPa, 241 kPa and 310 kPa by Huang et al. (2009a). Figure 8 presents the comparisons of predicted and measured shear stress-strain behaviour of fresh ballast. A good agreement can be found between the DEM predictions and the experimental results. There was strain hardening at the highest normal stress of 310 kPa, which was well predicted by the DEM simulation. At lower normal stresses, the experimental data of Huang et al. (2009a) indicated strain softening. Except for the lowest normal stress of 172 kPa, where the DEM prediction tended to overestimate the shear stress, the strain softening behaviour for  $\sigma_n = 241$  kPa shows an acceptable agreement between the numerical simulation and test data. As Lackenby et al. (2007) explained, particle breakage and associated load drop can be significant at low normal or confining stress levels, but for the laboratory data in particular, the drop in shear stress at a shear strain of 4-6% may be attributed to some degradation of the particles.

## DEM simulation for fouled ballast

Huang et al. (2009b) and Huang and Tutumluer (2011) presented a method to simulate fouled ballast in DEM by reducing the inter-particle coefficient of friction. This method is capable of capturing the stress-strain behaviour of fouled ballast within a reasonable computational time frame, but it did not examine the volumetric changes (either dilation or compression) of ballast at varying levels of fouling. Some studies, including Ni et al. (2000) and Lu and McDowell (2008), suggested that depending on the extent to which inter-particle friction was reduced, the granular assembly could undergo less dilation. The tendency to dilate is also a function of the initial distribution of particle sizes, initial compacted density, degree of fouling, applied confining pressure, and the rate of particle breakage, among others. In this study, the extent of dilation for the type of ballast and gradation given was predominantly a function of normal stress and to a lesser extent, by the degree of fouling (Figure 9). For a level of fouling less than VCI=40%, the maximum dilation at a given normal stress was relatively unaffected, while dilation at higher levels of fouling increased slightly. This was not surprising because when compacted, coal fouling is relatively incompressible, but during shearing at high VCI, the coal fines that fill the voids may impede the grains of ballast from re-packing and thereby promote dilation. Apart from decreasing the pore space between the grains of ballast, compacted coal fouling may even dilate itself and force the ballast to segregate and dilate.

## Proposed method for modelling fouled ballast in DEM

Fouling is caused by fine particles that accumulate in the voids of ballast. Therefore, fouled ballast should ideally be simulated in DEM by injecting various amounts of fine particles into the voids to represent different values of VCI (Figure 10a). Owing to fouling material between the individual rough and angular particles of ballast, the inter-particle friction angle is expected to decrease (Figure 10b). This reduction in the apparent angle of friction was evaluated experimentally and presented in Figure 11 showing increasing normal stress. This reduction of the inter-particle coefficient of friction ( $\mu$ ) in DEM was approximately determined based on the decrease in the apparent angle of friction of fouled ballast measured experimentally, as shown in Figure 11. In this DEM study, coal fines were simulated by 1.5mm spheres, which was similar to  $d_{50}$  of coal fines conducted in the laboratory, generated within the voids of ballast.. The values of

normal and shear stiffness ( $k_n$  and  $k_s$ ) required for the DEM analysis are always difficult to determine correctly, so in order to obtain some acceptable values of  $k_n$  and  $k_s$ , a conventional shear box test (60mm  $\times$  60mm  $\times$  25mm) was conducted on compacted coal fouling with a density of 1280kg/m<sup>3</sup>. By varying the  $k_n$  and  $k_s$  values in the DEM simulation to match the shear stress-strain plots obtained for direct shear testing,  $k_n=k_s=1.27 \times 10^4$  N/m was found to be appropriate. The relevant micro-mechanical parameters ( $k_n$ ,  $k_s$ ,  $\mu$ ) for varying the VCI are shown in Table 2, where the increased VCI is represented by an increased number of small spheres that mimic the fouling particles.

Large scale direct shear of fouled ballast at three different normal stresses of 15 kPa, 27 kPa, and 75 kPa were simulated using DEM. Figures 12-14 show the comparisons between DEM simulation and experimental results where VCI=20%, 40%, and 70%, respectively. It is evident that the shear stress-strain curves predicted by DEM simulation generally agree with those measured experimentally. The DEM simulation also predicted that the ballast would soften under strain at all levels of fouling and dilate significantly when the shear strain exceeded 5% which may also attribute to the rigidity of loading plate. As expected, the peak shear stress decreased with an increase in VCI at every level of applied normal stress. As mentioned earlier, coal fouling would reduce the inter-particle friction of fresh ballast by coating the surfaces of rough aggregates, causing a reduction in shear strength. All the samples were compressed at the beginning of the test, followed by significant dilation. This was expected from dense granular materials that normally indicate strain softening at high rates of dilation. At a relatively low applied normal stress (15 kPa), dilation occurred almost from the beginning of shearing, whereas significantly less dilation occurred at the highest applied normal stress ( $\sigma_n = 75 \text{ kPa}$ ).

Not surprisingly, there is some disparity in volumetric strains between the numerical predictions and laboratory data. This can be attributed to differences in particle angularity between the DEM simulation and laboratory observations, as well as particle degradation not considered in the current DEM analysis. McDowell et al. (2006) also observed similar differences in volumetric strain between DEM and experimental data for tri-axial testing. Irrespective of the efforts made in DEM to clump particles together to mimic irregular or angular ballast used in real rail tracks, accurate representations of the sharp corners of blasted aggregates and their surface roughness will always remain a key challenge to the DEM modeller. Dilation that depends on size and

shape, and the nature of particle degradation depending on the applied stresses and shearing rates, will require further insight into micro-mechanical modelling to make further improvements in the DEM.

### **Distribution of Contact forces in fresh and fouled ballast**

Figure 15 shows the evolution of chains of contact force in fresh and fouled ballast at VCIs ranging from 0% to 70%, at a normal stress of 51 kPa. The maximum contact forces and number of contacts for each simulation in the assembly are shown in Figure 16. While the number of contacts increases significantly with an increased VCI, the maximum value of contact forces decreases with an increasing VCI. When there are coal fines in the voids, the applied load does not only transmit through the large aggregate skeleton but also across the fine coal particles. This results in a reduced maximum contact force magnitude corresponding to a higher number of particle contacts. Consequently, a more uniform distribution of stress is expected in the fouled ballast, as reflected by the distribution of a more dense contact force. The greater the VCI, the more prominent will be the corresponding uniform distribution of contact forces over a larger number of contacts, a result that may reduce ballast breakage by diminishing the intensity of stress concentrated in the fouled ballast matrix. These micro-mechanical observations obtained from DEM clearly explain the reduced breakage of fouled ballast compared to fresh ballast as measured experimentally.

### **Conclusions**

A series of DEM simulations that captured three-dimensional shaped ballast in direct shear tests, were conducted on fresh and fouled ballast at various levels of fouling, to study the volumetric change and corresponding stress-strain behaviour of this granular assembly. These irregularly shaped particles of ballast were simulated by overlapping spherical particles using the clump logic of PFC<sup>3D</sup>. The coal fines were modelled by introducing a specified number of fine spherical particles into the ballast voids. The degree of fouling was defined by the Void Contaminant Index (VCI) that was varied from 20% to 70%. For a given normal stress ( $\sigma_n$ ) and VCI, the DEM model captured the shear stress-strain response and volumetric changes observed in the

laboratory experiments. As expected, the highest peak shear stress occurred in fresh ballast, but it decreased consistently with an increase in VCI for a given value of normal stress.

The DEM simulation indicated that coal fines would reduce the shear strength and increase the dilation of fouled ballast at relatively high levels of VCI (>60%). Dilation was highest at the lowest values of normal stress ( $\sigma_n = 15 \text{ kPa}$ ). It was shown that the volumetric dilation predicted by DEM was somewhat higher than the dilation actually measured. This can be attributed to the inevitable variations in particle angularity between the DEM model and actual ballast, as well as any particle degradation that was not considered in the numerical analysis and simulation of one rigid loading plate. The drop in peak shear stress and increased compression in the laboratory at shear strains of 5-7% also supports the view that particle degradation can have a significant influence. Even with small quantities, the coal fines coat the grains of ballast and reduce the surface roughness (i.e. role of lubricant), while at increased VCI the coal fines inhibit the ballast from repacking by forming a compacted layer between the aggregates. Therefore, apart from a decrease in shear strength as a result of reduced inter-particle friction, coal fines at high VCI values can also increase the dilation of the fouled ballast, especially at low normal stresses. So by taking advantage of the DEM simulation technique, the internal distribution of contact forces and displacement of the particles could be examined. Such micro-mechanical observations enable us to insightfully appreciate the evolution of volumetric changes and corresponding shear strength during geotechnical laboratory processes, which is currently not possible through FEM and other continuum mechanic approaches. The more uniform contact force distributions attributed to increased overall particle contact area of fouled ballast justify the reduced breakage as observed in the laboratory. Although the current DEM analysis did not consider ballast breakage, the numerical predictions of stress-strain behaviour at various levels of fouling and normal levels of stress were in acceptable agreement with the experimental observations of direct shear test.

## Acknowledgement

The authors are grateful for the financial support provided by CRC for Rail Innovation. The laboratory assistance from Mr. Alan Grant is also appreciated.

## Notation

$B$	width of the shear box
$d_{100}$	maximum particle size
$e_b$	void ratio of fresh ballast
$e_f$	void ratio of fouling material
$F_N$	normal force at the shear band
$F_S$	shear force at the shear band
$G_{s,b}$	specific gravity of ballast
$G_{s,f}$	specific gravity of fouling material
$k_n$	contact normal stiffness
$k_{n-wall}$	contact normal stiffness of wall-particle
$k_s$	contact shear stiffness
$k_{s-wall}$	contact shear stiffness of wall-particle
$L$	length of the shear box
$M_f$	dry mass of fouling material
$M_b$	dry mass of fresh ballast

$N$	applied normal load
$N_{Y_{iw}}$	normal force acting on the left and right side walls of the upper box
$S_{Y_{iw}}$	shear force acting on the upper box
$v$	shear velocity
VCI	Void Contamination Index
$W_b$	weight of ballast in upper box
$W_p$	weight of the top load plate
$t$	shearing time
$\varepsilon_s$	shear strain
$\mu$	inter-particle coefficient of friction
$\sigma_n$	normal stress
$\tau_{zy}$	shear stress
$\phi_b$	bulk coefficient of friction

Accepted Manuscript  
Not Copyedited

## References

- Anderson, W. F. & Fair, P. (2008). Behavior of railroad ballast under monotonic and cyclic loading. *Journal of Geotechnical and Geoenvironmental Engineering*. 143(3): pp.316–327.
- Aursudkij, B., McDowell, G. R. & Collop, A. C. (2009). Cyclic loading of railway ballast under triaxial conditions and in a railway test facility. *Granular Matter*. 11: pp.391–401.
- Charles, J. A. & Watts, K. S. (1980). The influence of confining pressure on the shear strength of compacted rockfill. *Géotechnique*. 30(4): pp.353-367.
- Cui, L. & O'Sullivan, C. (2006). Exploring the macro- and micro-scale response of an idealised granular material in the direct shear apparatus. *Géotechnique*. 56(7): pp.455-468.
- Cundall, P. A. & Strack, O. D. L. (1979). A discrete numerical model for granular assemblies. *Géotechnique*. 29(1): pp.47-65.
- Dombrow, W., Huang, H. & Tutumluer, E. (2009). Comparison of coal dust fouled railroad ballast behavior- granite vs. limestone. *Bearing Capacity of Roads, Railways and Airfields, Proceedings of the 8th International Conference (BCR2A'09)*. Taylor & Francis Group.
- Fagnoul, A. & Bonnechere, F. (1969) Shear strength of porphyry materials. *Proceedings of the 7<sup>th</sup> International Conference on Soil Mechanics and Foundation Engineering*. Mexico.
- Feldman, F. & Nissen, D. (2002). Alternative testing method for the measurement of ballast fouling. *Conference on Railway Engineering*. RSTA, Wollongong.
- Ferrellec, J. F. & McDowell, G. R. (2008). A simple method to create complex particle shapes for DEM. *Geomechanics and Geoengineering*. 3(3): pp.211 — 216.
- Hossain, Z., Indraratna, B., Darve, F. & Thakur, P. K. (2007). DEM analysis of angular ballast breakage under cyclic loading. *Geomechanics and Geoengineering*. 2(3): pp.175-181.
- Huang, H., Tutumluer, E., & Dombrow, W. (2009a). Laboratory characterisation of fouled railroad ballast behavior. *88th Annual Meeting of the Transportation Research Board*. Washington, DC.

Huang, H., Tutumluer, E., Hashash, Y. M. A., & Ghaboussi, J. (2009b). Discrete element modeling of aggregate behavior in fouled railroad ballast. *Geotechnical Special Publication 192, ASCE*: pp.33-41.

Huang, H. & Tutumluer, E. (2011). Discrete Element Modeling for fouled railroad ballast. *Construction and Building Materials*. 25: pp.3306-3312.

Indraratna, B., Wijewardena, L.S.S. & Balasubramaniam, A. S. (1993). Large-scale triaxial testing of greywacke rockfill. *Géotechnique*: 42(1): pp.37-51.

Indraratna, B., Ionescu, D. & Christie, D. (1998). Shear behaviour of railway ballast based on Large Scale Triaxial Testing. *Journal of Geotechnical and Geoenvironmental Engineering, ASCE*. 124(5): 439-449.

Indraratna, B. & Salim, W. (2002). Modelling of particle breakage of coarse aggregates incorporating strength and dilatancy. *Geotechnical Engineering, Proceedings of Institution of Civil Engineers, UK*. 155(4): pp.243-252

Indraratna, B., Lackenby, J., & Christie, D. (2005). Effect of confining pressure on the degradation of ballast under cyclic loading. *Géotechnique*. 55(4): pp.325–328.

Indraratna, B., Nimbalkar, S. & Tennakoon, N. (2010b). The behaviour of ballasted track foundations: track drainage and geosynthetic reinforcement. *GeoFlorida 2010: Advances in Analysis, Modeling & Design (GSP 199)*. Florida.

Indraratna, B., Thakur, P. K. & Vinod, J. S. (2010a). Experimental and numerical study of railway ballast behavior under cyclic loading. *International Journal of Geomechanics, ASCE*. 10(4): pp.136-144.

Indraratna, B., Vinod, J. S. & Lackenby, J. (2009). Influence of particle breakage on the resilient modulus of railway ballast. *Géotechnique*. 59(7): pp.643–646.

Indraratna, B., Ngo, N. T., & Rujikiatkamjorn, C. (2011a). Behavior of geogrid-reinforced ballast under various levels of fouling. *Geotextiles and Geomembranes*. 29(3): pp.313-322.

- Itasca (2008). Particle flow code in three dimensions (PFC<sup>3D</sup>). *Itasca Consulting Group, Inc., Minnesota*.
- Lackenby, J., Indraratna, B., McDowell, G., & Christie, D. (2007). Effect of confining pressure on ballast degradation and deformation under cyclic triaxial loading. *Géotechnique*. 57(6): pp.527–536
- Lim, W. L., & McDowell, G. R. (2005). Discrete element modelling of railway ballast. *Granular Matter*. 7(1): pp.19-29.
- Liu, S. H. (2006). Simulating a direct shear box test by DEM. *Canadian Geotechnical Journal*. 43(2): pp. 155-168.
- Lobo-Guerrero, S, & Vallejo, L. E. (2006). Discrete element method analysis of railtrack ballast degradation during cyclic loading. *Granular Matter*. 8(3-4): pp.195-204.
- Lu, M., & McDowell, G. R. (2006). Discrete element modelling of ballast abrasion. *Géotechnique*. 56(9): pp.651-655.
- Lu, M., & McDowell, G. R. (2007). The importance of modelling ballast particle shape in the discrete element method. *Granular Matter*. 9(1-2): pp.69-80.
- Lu, M., & McDowell, G. R. (2008). Discrete element modelling of railway ballast under triaxial conditions. *Geomechanics and Geoengineering: An International Journal*. 3(4): pp.257-270.
- Marsal, R. J. (1973), Mechanical Properties of Rockfill. *In: Embankment Dam Engineering*. Wiley, New York, pp. 109-200.
- Marachi, N. D. (1969). Strength and deformation characteristics of rockfill materials. *PhD Thesis*. University of California.
- McDowell, G. R., Harireche, O., Konietzky, H., Brown, S. F., & Thom, N. H. (2006). Discrete element modelling of geogrid-reinforced aggregates. *Geotechnical Engineering* 159(GE1): pp.35-48.

Ni, Q., Powrie, W., Zhang, X., & Harkness, R. (2000). Effect of particle properties on soil behaviour: 3-D numerical modelling of shearbox test. *Geotechnical Special Publication 96, ASCE*: pp.58-70.

Oda, M., & Iwashita, K. (1999). *Mechanics of granular materials: An introduction*. Rotterdam: A. A. Balkema.

O'Sullivan, C., Cui, L., & O'Neill, S. C. (2008). Discrete element analysis of the response of granular materials during cyclic loading. *Soils and Foundations*. 48(4): pp:511-530

O'Sullivan C., & Cui, L. (2009). Micromechanics of granular material response during load reversals: Combined DEM and experimental study. *Powder Technology*. 193: pp:289-302

O'Sullivan C. (2011). *Particulate Discrete Element Modelling: A Geomechanics Perspective*. Spon Press, London.

Selig, E. T. & Waters, J. M. (1994). *Track geotechnology and substructure management*. Thomas Telford, London.

Sitharam, T. G., & Vinod, J. S. (2005). Shear behavior of glass beads using DEM. *Proceedings of the 5th International Conference on Micromechanics of Granular Media (Vol.1)*. Stuttgart, Germany.

Sitharam, T. G., & Vinod, J. S. (2008). Numerical simulation of liquefaction and pore pressure generation in granular materials using DEM. *International Journal of Geotechnical Engineering*. 2(2): pp.103-113.

Sitharam, T. G., & Vinod, J. S. (2009). Critical state behaviour of granular materials from isotropic and rebounded paths: DEM simulations. *Granular Matter*. 11(1): pp.33-42.

Stahl, M., & Konietzky, H. (2011). Discrete element simulation of ballast and gravel under special consideration of grain-shape, grain size and relative density. *Granular Matter*. 13(4):pp.417-428.

Suiker, A. S. J., Selig, E. T., & Frenkel, R. (2005). Static and cyclic triaxial testing of ballast and subballast. *Journal of Geotechnical and Geoenvironmental Engineering Computations*. 131(6): pp.771–782.

Thakur, P. K., Vinod, J. S., & Indraratna, B. (2010). Effect of particle breakage on cyclic densification of ballast: A DEM approach. *Materials Science and Engineering*. 10: pp.1-7.

Tutumluer, E., Huang, H., Hashash, Y., & Ghaboussi, J. (2007). Discrete element modeling of railroad ballast settlement. *Proceedings of the AREMA 2007 Annual Conference*. Chicago, IL, USA.

Tutumluer, E., Dombrow, W., & Huang, H. (2008). Laboratory characterization of coal dust fouled ballast behavior. *Proceedings of the AREMA 2008 Annual Conference*. Salt Lake City, UT, USA.

Wang, J., Dove, J. E., & Gutierrez, M. S. (2007). Discrete-continuum analysis of shear banding in the direct shear test. *Géotechnique*. 57(6): pp. 513–526.

Zhang, L. & C. Thornton (2007). A numerical examination of the direct shear test. *Géotechnique*. 57(4): pp.343–354.

### **List of Tables**

Table 1. Micro-mechanical parameters adopted for ballast and shear box boundary walls in DEM

Table 2. Micro-mechanical parameters adopted for coal fines to simulate fouled ballast at a specific VCI

Accepted Manuscript  
Not Copyedited

Table 1. Micro-mechanical parameters adopted for ballast and shear box boundary walls in DEM

Micromechanical parameters	Values
Contact normal stiffness $k_n$ (N/m)	$0.52 \times 10^8$
Contact shear stiffness $k_s$ (N/m)	$0.52 \times 10^8$
Inter-particle coefficient of friction $\mu$	0.8
Contact normal stiffness of wall-particle, $k_{n-wall}$ (N/m)	$1 \times 10^8$
Shear stiffness of wall of wall-particle, $k_{s-wall}$ (N/m)	$1 \times 10^8$
Particle density ( $\text{kg/m}^3$ )	2700

Table 2. Micro-mechanical parameters adopted for coal fines to simulate fouled ballast at a specific VCI

VCI (%)	Contact normal stiffness, $k_n$ (N/m)	Contact shear stiffness, $k_s$ (N/m)	Inter-particle coefficient of friction of coal fine, $\mu$	Number of added balls to simulate fouling	$V_{\text{fines}}/V_{\text{ballast}}$	Inter-particle coefficient of friction of fouled ballast assembly
20	$1.27 \times 10^4$	$1.27 \times 10^4$	0.2	72,833	0.107	0.72
40	$1.27 \times 10^4$	$1.27 \times 10^4$	0.2	145,665	0.214	0.65
70	$1.27 \times 10^4$	$1.27 \times 10^4$	0.2	252,113	0.370	0.58

Accepted Manuscript  
Not Copyedited

## List of Figures

Figure 1. Particle size distribution of fresh and fouled ballast at VCIs varying from 20% to 70%VCI, conducted in the laboratory

Figure 2. Library of ballast particle shapes used in PFC<sup>3D</sup>

Figure 3. Initial assembly of large-scale direct shear test with irregular shaped particles, (a) fresh ballast and (b) 40%VCI fouled ballast

Figure 4. Schematic diagram of forces acting in the direct shear box (not to scale)

Figure 5. Comparisons between the DEM simulation and experiment for fresh ballast at 3 normal stresses of  $\sigma_n = 27\text{kPa}$ ,  $51\text{kPa}$ , and  $75\text{kPa}$ , (a) shear stress versus shear strain, (b) volumetric strain versus shear strain

Figure 6. Distribution of contact forces (projection of all contact forces on vertical plane YZ) in fresh ballast for a normal stress of  $51\text{ kPa}$ , (a) at shear strain  $\epsilon_s = 0\%$ , (b) at shear strain  $\epsilon_s = 3\%$ , (c) at shear strain  $\epsilon_s = 6\%$ , (d) at shear strain  $\epsilon_s = 13\%$

Figure 7. Displacement vectors of particles in the shear box for a normal stress of  $51\text{ kPa}$ , (a) at a shear strain  $\epsilon_s = 3\%$ , (b) at a shear strain  $\epsilon_s = 13\%$  and (c) a schematic diagram of the conceptual movement of ballast particles in direct shear testing

Figure 8. Comparisons of shear stress – shear strain between a DEM simulation and an experiment of a large-scale direct shear test for fresh ballast, as reported by Huang et al. (2009a)

Figure 9. The variation in maximum dilation (at the end of shearing) of fouled ballast with various VCIs ranging from 0% to 95%, measured experimentally by the authors

Figure 10. A combined method for modelling fouled ballast, (a) small spherical balls added to simulate fouled ballast, (b) inter-particle coefficient of friction reduced to simulate fouled ballast

Figure 11. Effect of VCI on the apparent angle of shearing resistance of fouled ballast, measured experimentally by the Authors authors

Figure 12. Comparisons between the DEM simulation and experiment for 20%VCI fouled ballast at 3 normal stresses of  $\sigma_n = 15$  kPa, 27 kPa, and 75 kPa, (a) shear stress versus shear strain, (b) volumetric strain versus shear strain

Figure 13. Comparisons between the DEM simulation and experiment for 40%VCI fouled ballast at 3 normal stresses of  $\sigma_n = 15$  kPa, 27 kPa, and 75 kPa, (a) shear stress versus shear strain, (b) volumetric strain versus shear strain

Figure 14. Comparisons between the DEM simulation and experiment for 70%VCI fouled ballast at 3 normal stresses of  $\sigma_n = 15$  kPa, 27 kPa, and 75 kPa, (a) shear stress versus shear strain, (b) volumetric strain versus shear strain

Figure 15. Evolution of the distribution of contact forces (projection of all contact forces on vertical plane YZ) in fresh and fouled ballast at various VCIs (at 3% shear strain), (a) 0% VCI, (b) 20%VCI, (c) 40% VCI and (d) 70% VCI

Figure 16. Variation of the number of contacts, and the maximum contact force for fresh and fouled ballast at various VCIs ranging from 0% to 70%, at 3% shear strain

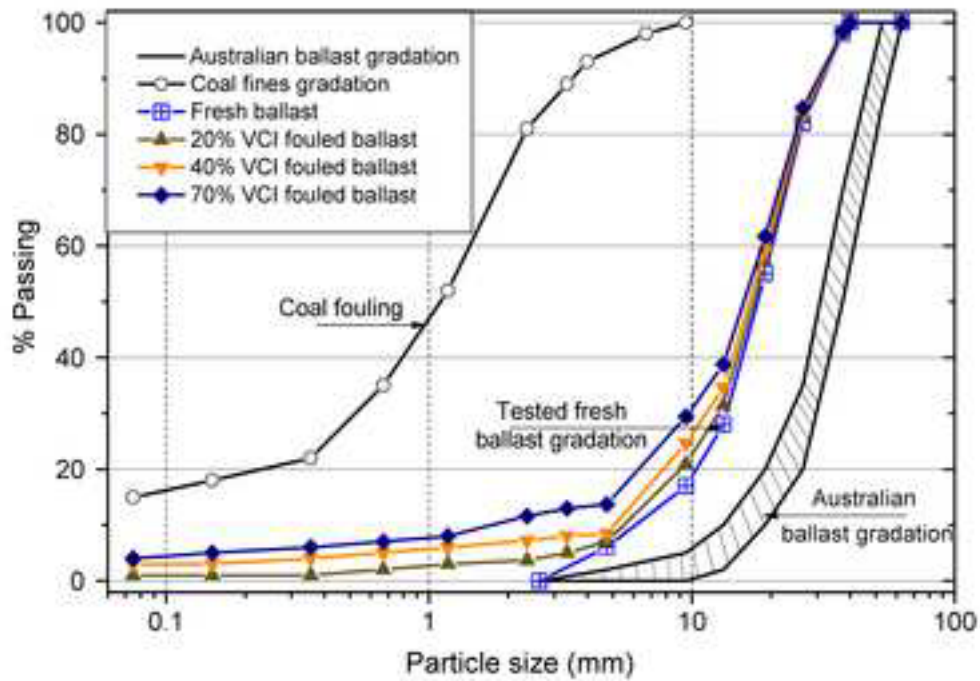
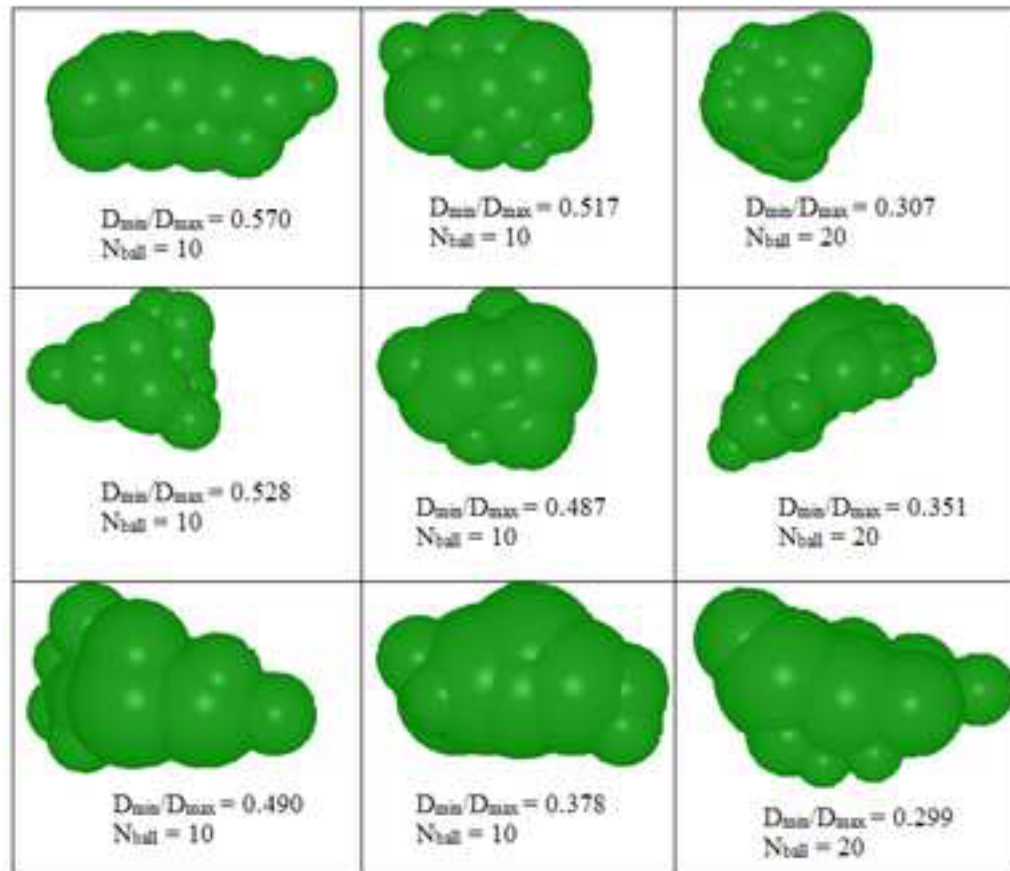


Figure 1. Particle size distribution of fresh and fouled ballast at VCIs varying from 20% to 70%VCI, conducted in the laboratory

Accepted Manuscript  
 Not Copyedited



$D_{min}/D_{max}$ : ratio of the dimension of smallest ball divided by dimension of largest ball in each clump

$N_{ball}$ : number of spherical balls in each clump

Figure 2. Library of ballast particle shapes used in PFC<sup>1D</sup>

Accepted Manuscript  
Not Copyedited

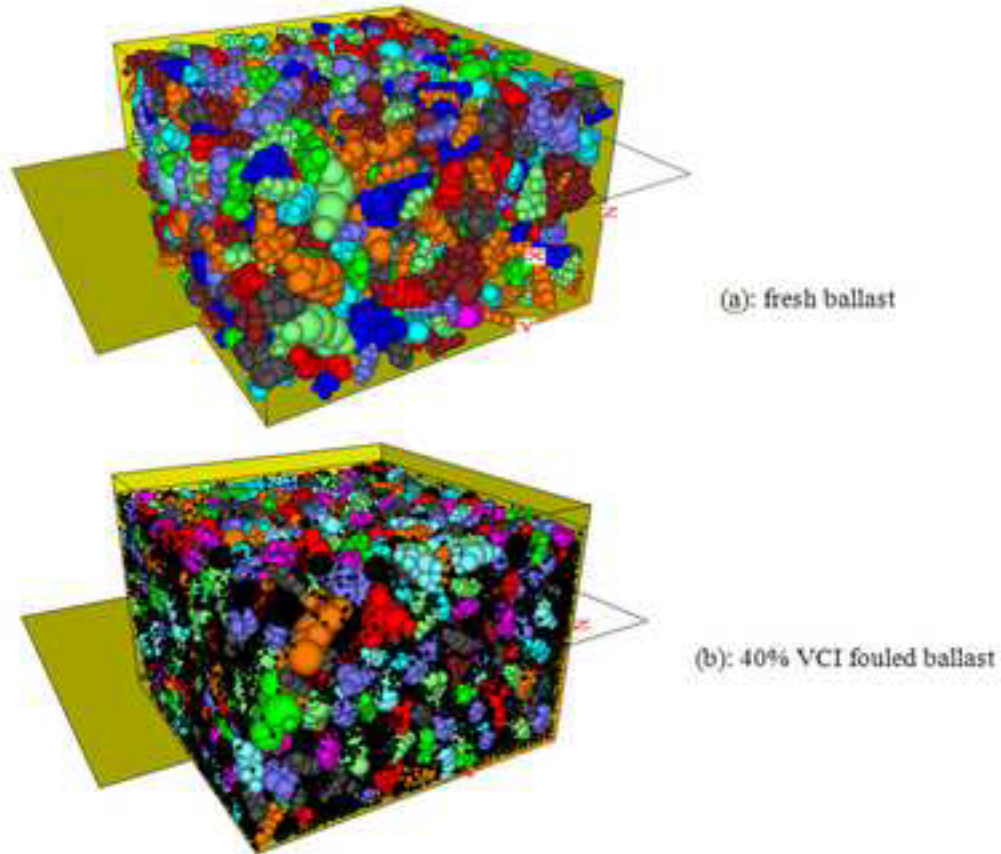


Figure 3. Initial assembly of large-scale direct shear test with irregular shaped particles, (a) fresh ballast and (b) 40%VCI fouled ballast

Accepted Manuscript  
Not Copyedited



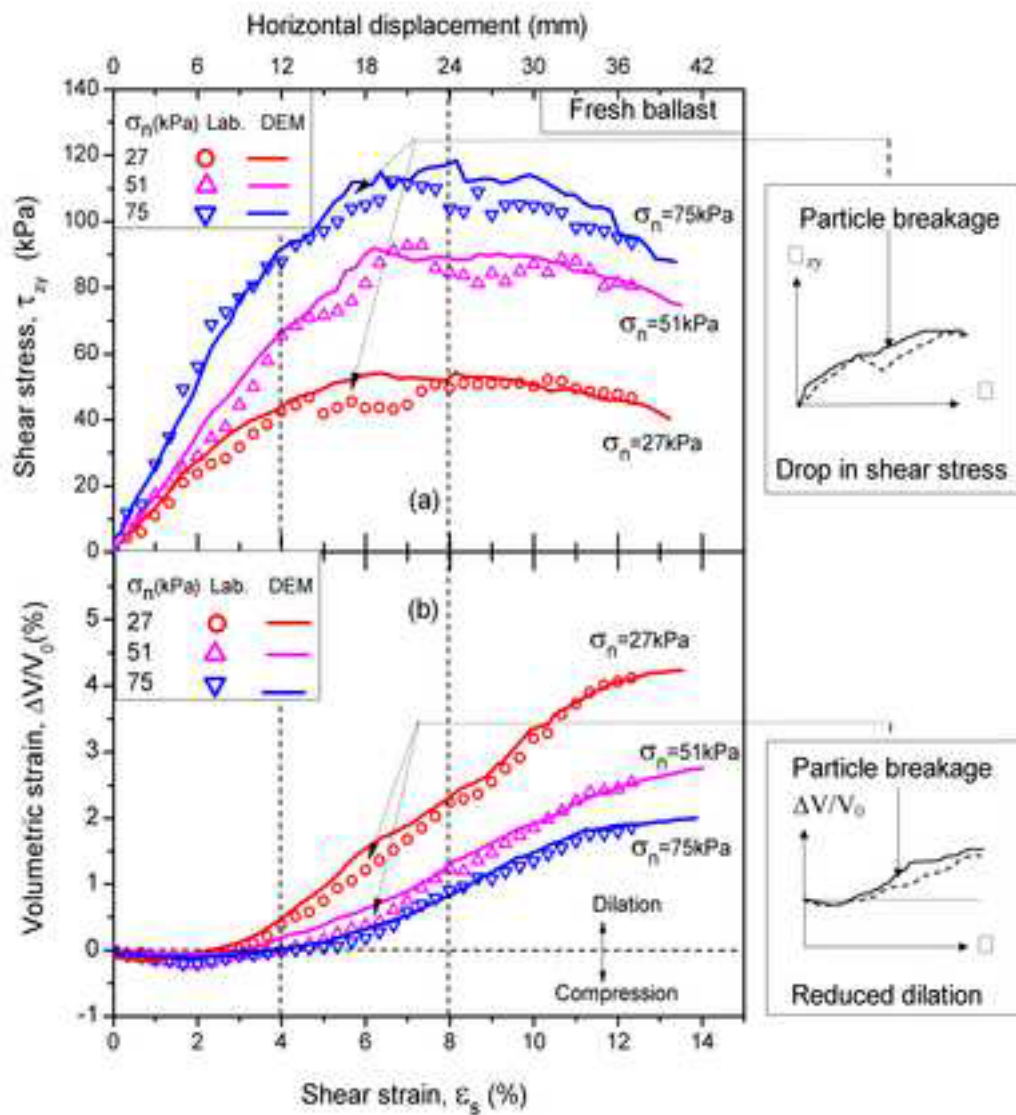


Figure 5. Comparisons between the DEM simulation and experiment for fresh ballast at 3 normal stresses of  $\sigma_n = 27$  kPa, 51 kPa, and 75 kPa, (a) shear stress versus shear strain, (b) volumetric strain versus shear strain

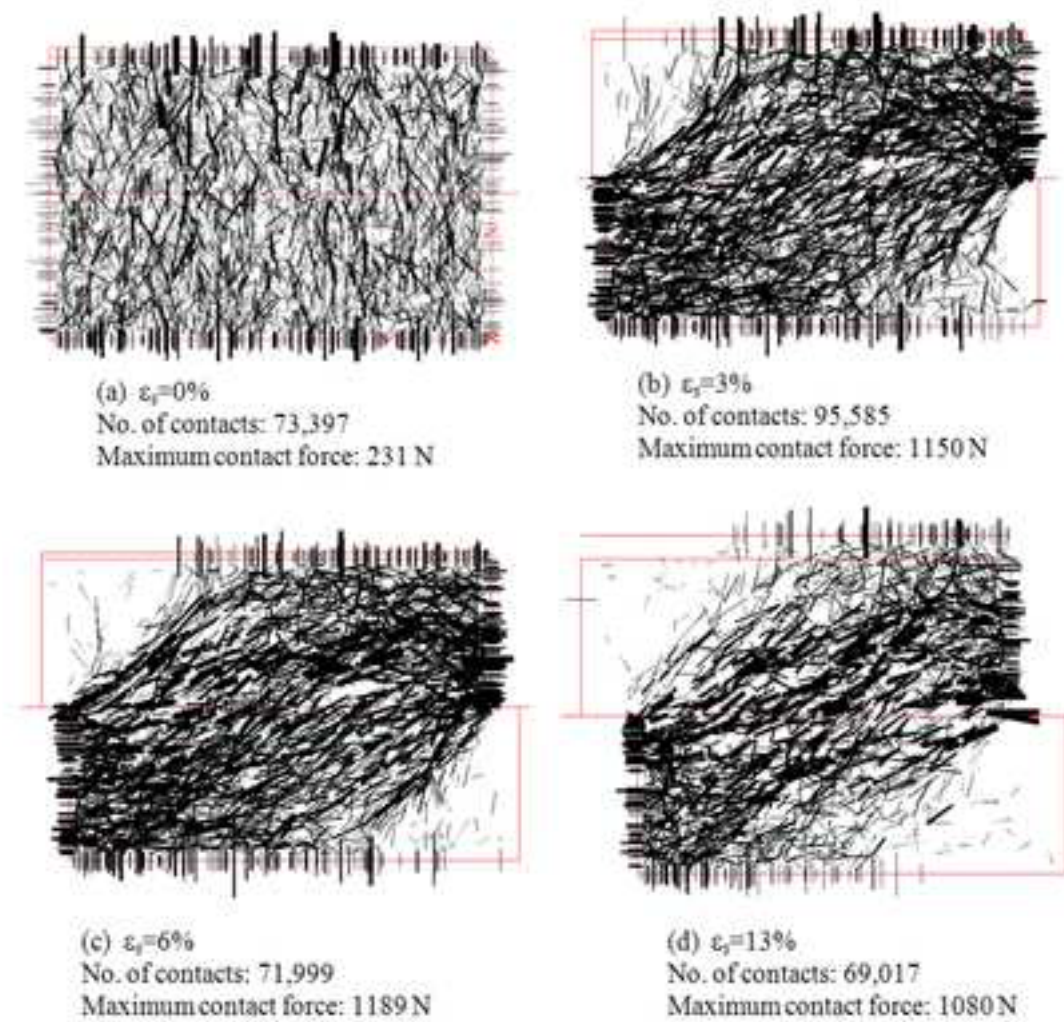


Figure 6. Distribution of contact forces (projection of all contact forces on vertical plane YZ) in fresh ballast for a normal stress of 51 kPa, (a) at shear strain  $\varepsilon_s = 0\%$ , (b) at shear strain  $\varepsilon_s = 3\%$ , (c) at shear strain  $\varepsilon_s = 6\%$ , (d) at shear strain  $\varepsilon_s = 13\%$

Accepted Manuscript  
 Not Copied

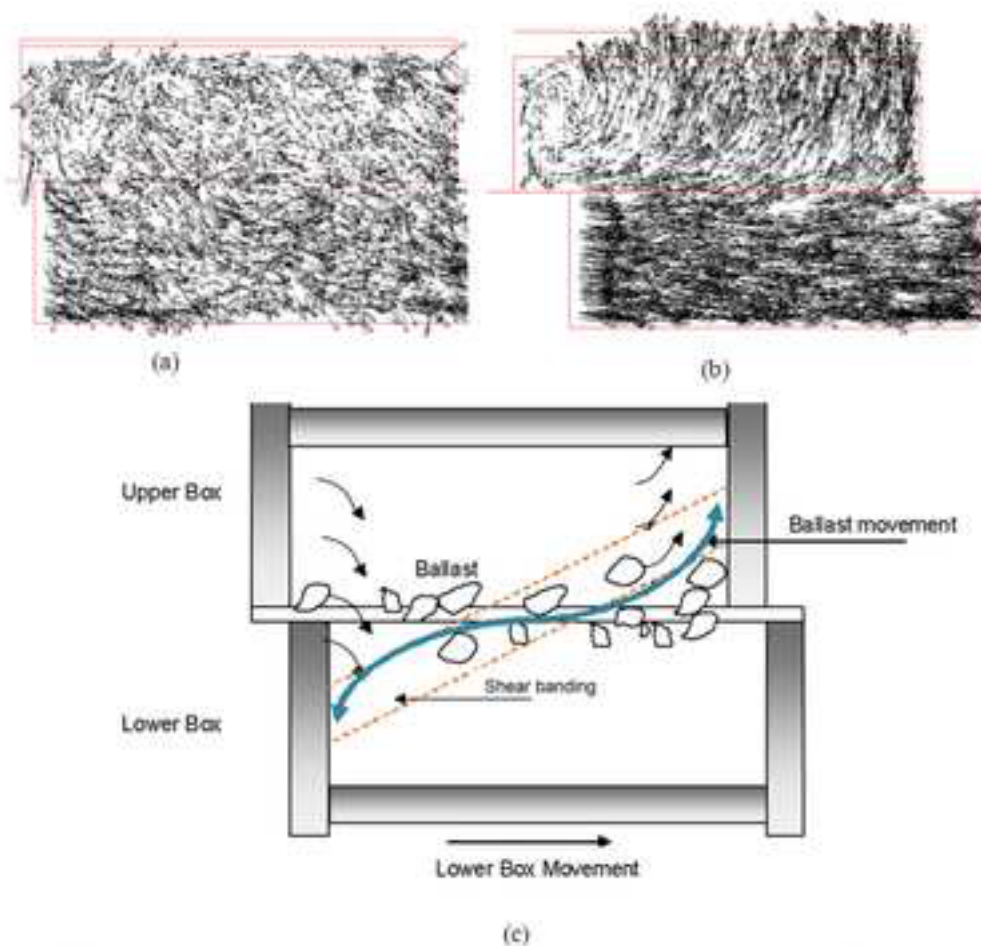


Figure 7. Displacement vectors of particles in the shear box for a normal stress of 51 kPa, (a) at a shear strain  $\epsilon_s = 3\%$ , (b) at a shear strain  $\epsilon_s = 13\%$  and (c) a schematic diagram of the conceptual movement of ballast particles in direct shear testing

Accepted Manuscript  
Not Copied

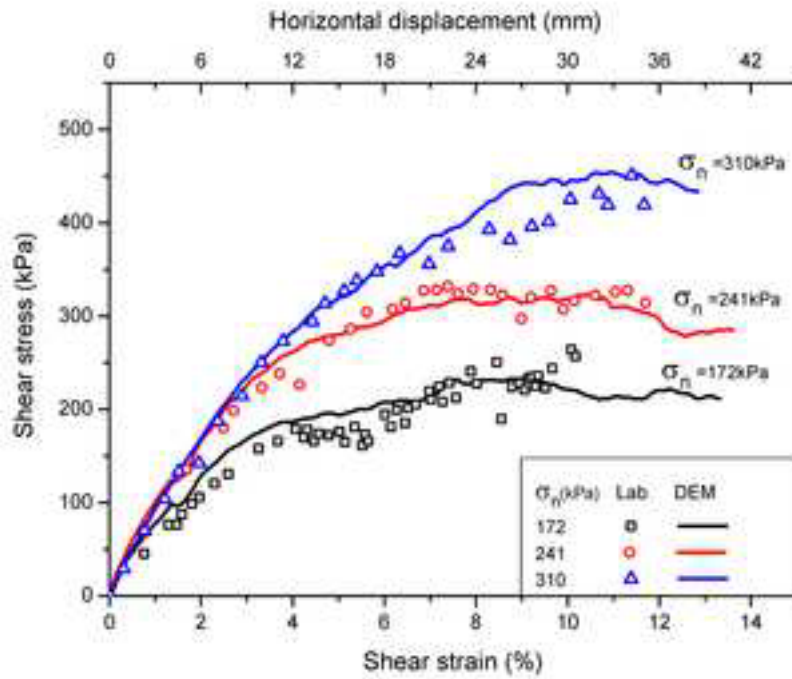


Figure 8. Comparisons of shear stress – shear strain between a DEM simulation and an experiment of a large-scale direct shear test for fresh ballast, as reported by Huang et al. (2009a)

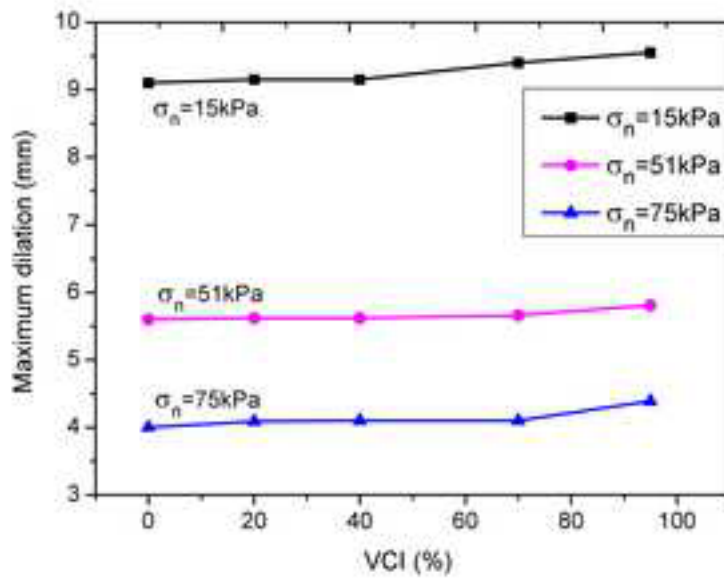
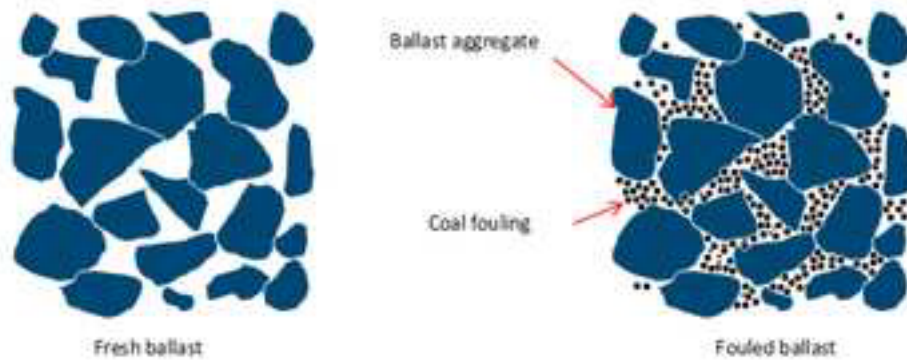
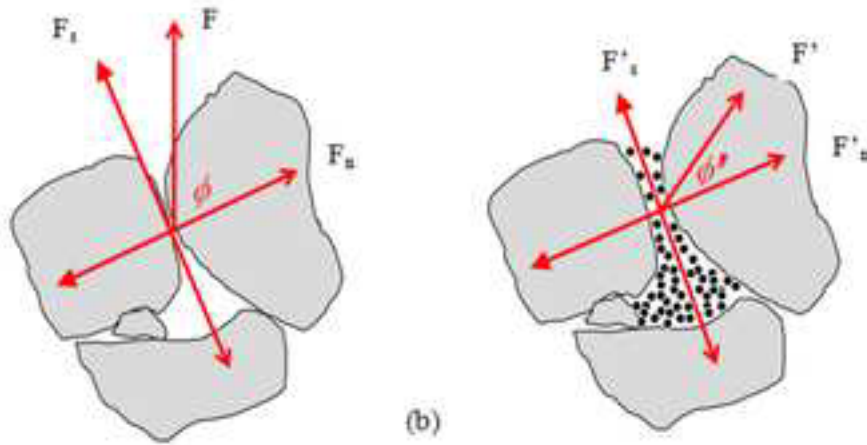


Figure 9. The variation in maximum dilation (at the end of shearing) of fouled ballast with various VCIs ranging from 0% to 95%, measured experimentally by the Authors

Accepted Manuscript  
Not Copyedited



(a) small spherical balls added to simulate fouled ballast



Fresh ballast, inter-particle friction angle  $\phi$

Fouled ballast, inter-particle friction angle  $\phi'$

Figure 10. A combined method for modelling fouled ballast, (a) small spherical balls added to simulate fouled ballast, (b) inter-particle coefficient of friction reduced to simulate fouled ballast

Accepted Manuscript  
Not Copyedited

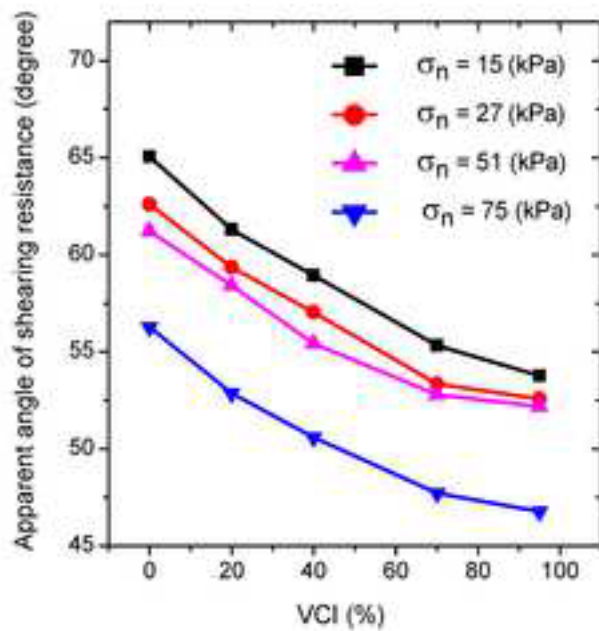


Figure 11. Effect of VCI on the apparent angle of shearing resistance of fouled ballast, measured experimentally by the authors

Accepted Manuscript  
 Not Copyedited

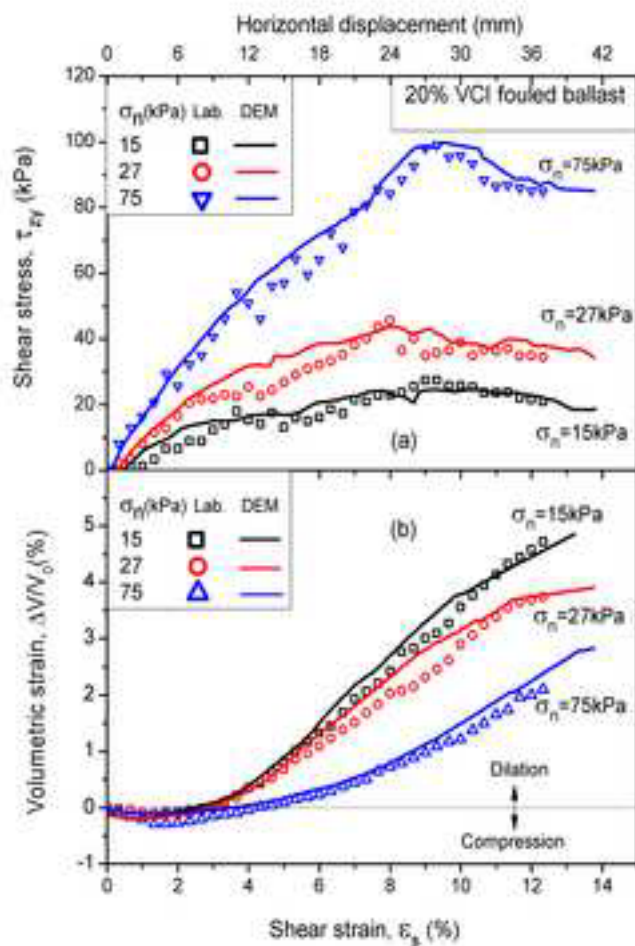


Figure 12. Comparisons between the DEM simulation and experiment for 20%VCI fouled ballast at 3 normal stresses of  $\sigma_n = 15$  kPa, 27 kPa, and 75 kPa, (a) shear stress versus shear strain, (b) volumetric strain versus shear strain

Accepted Manuscript  
Not Copied

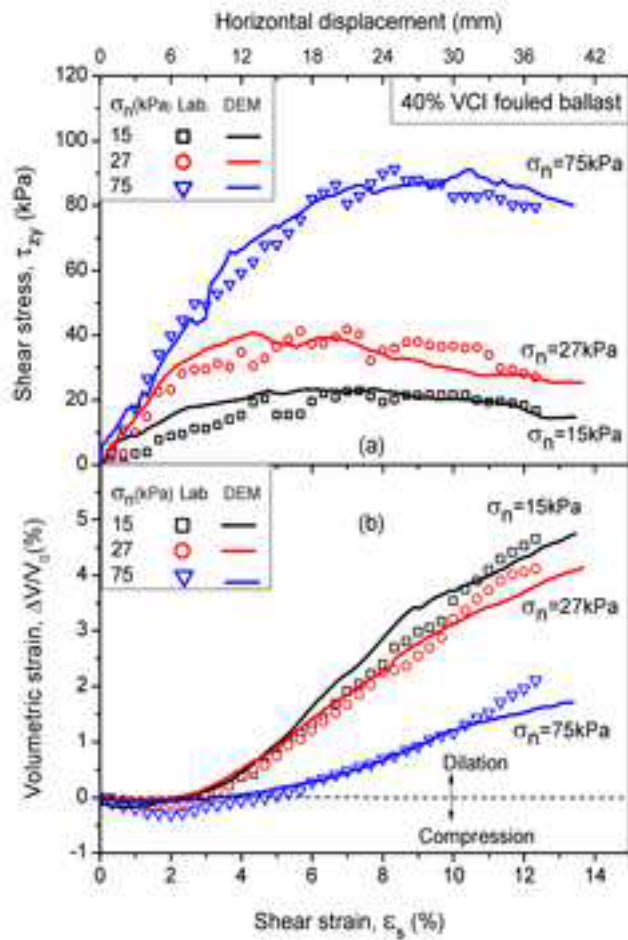


Figure 13. Comparisons between the DEM simulation and experiment for 40%VCI fouled ballast at 3 normal stresses of  $\sigma_n = 15$  kPa, 27 kPa, and 75 kPa, (a) shear stress versus shear strain, (b) volumetric strain versus shear strain

Accepted Manuscript  
Not Copied

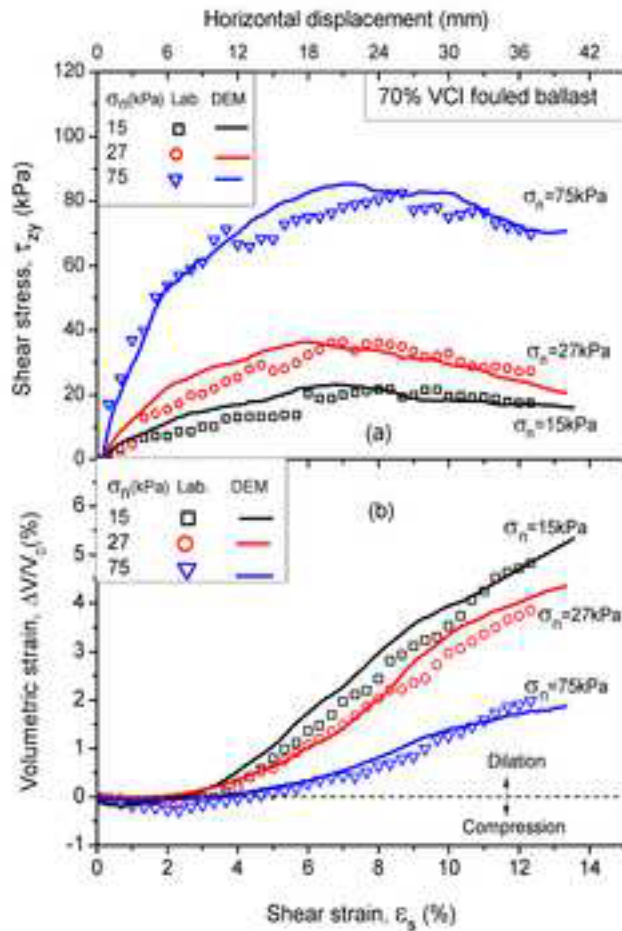


Figure 14. Comparisons between the DEM simulation and experiment for 70%VCI fouled ballast at 3 normal stresses of  $\sigma_n = 15$  kPa, 27 kPa, and 75 kPa, (a) shear stress versus shear strain, (b) volumetric strain versus shear strain

Accepted Manuscript  
Not Copied

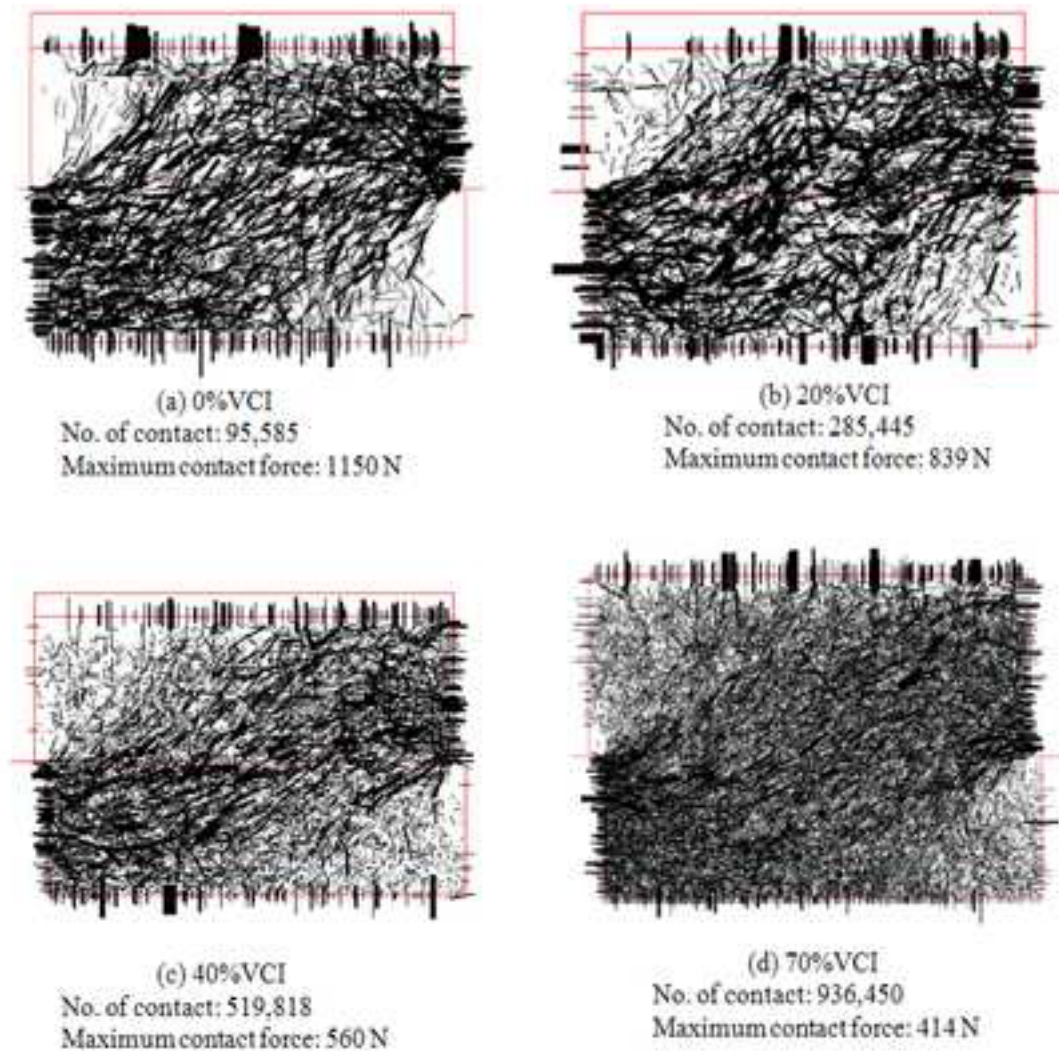


Figure 15. Evolution of the distribution of contact forces (projection of all contact forces on vertical plane YZ) in fresh and fouled ballast at various VCIs (at 3% shear strain), (a) 0% VCI, (b) 20%VCI, (c) 40% VCI and (d) 70% VCI

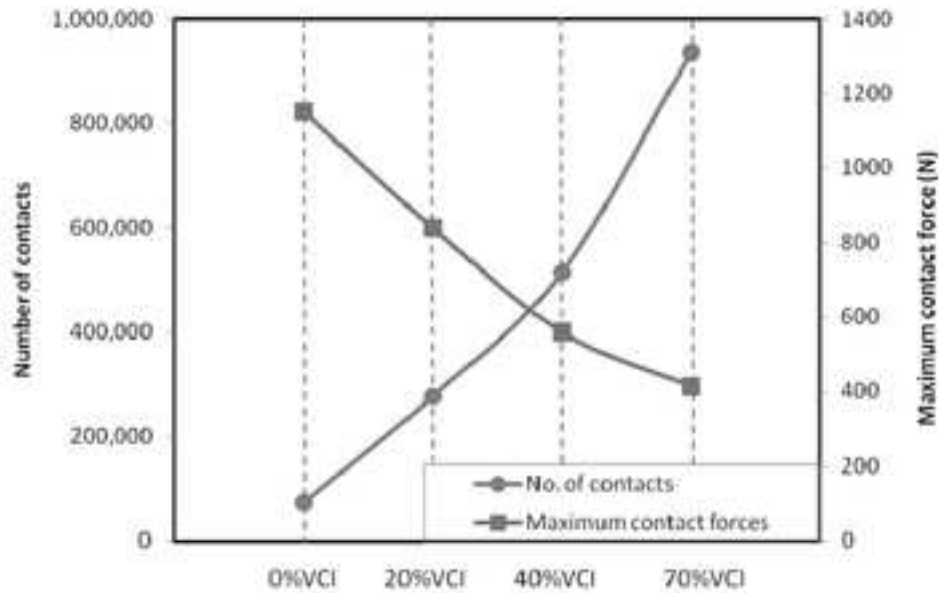


Figure 16. Variation of the number of contacts, and the maximum contact force for fresh and fouled ballast at various VCIs ranging from 0% to 70%, at 3% shear strain

Accepted Manuscript  
 Not Copyedited